How to dope the basal plane of 2H-MoS2 to boost the hydrogen evolution reaction?

Nawras Abidi, Audrey Bonduelle-Skrzypczak, Stephan Steinmann

Graphical Abstract

How to Dope the Basal Plane of 2H-MoS_2 to Boost the Hydrogen Evolution Reaction?

Nawras Abidi, Audrey Bonduelle-Skrzypczak, Stephan N. Steinmann

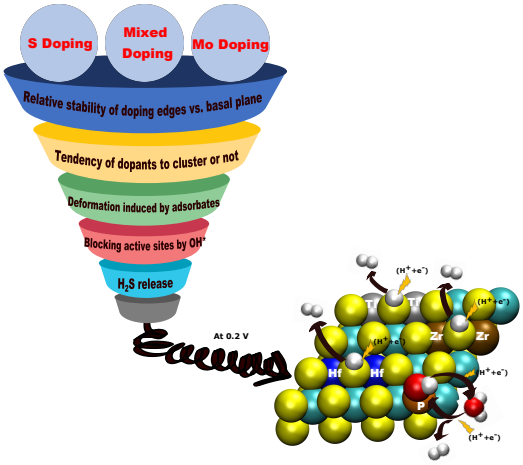

Highlights

How to Dope the Basal Plane of 2H-MoS_2 to Boost the Hydrogen Evolution Reaction?

Nawras Abidi, Audrey Bonduelle-Skrzypczak, Stephan N. Steinmann

- Extensive screening of non-noble metal substitutional doping of MoS_2 for activating the basal plane for the hydrogen evolution reaction (HER)
- Grand-canonical DFT is used for a realistic description of HER
- Only four systems out of seventy have been identified as promising (stable, feasible and active): doping with titanium, zirconium and hafnium, as well as a mixed sulfide/phosphide.

How to Dope the Basal Plane of 2H-MoS_2 to Boost the Hydrogen Evolution Reaction?

Nawras Abidi[a], Audrey Bonduelle-Skrzypczak[b], Stephan N. Steinmann[a]

[a] *Univ Lyon Ens de Lyon CNRS UMR 5182 Laboratoire de Chimie F69342 Lyon France*
[b] *IFP Energies nouvelles Rond-point de l'"'echangeur de Solaize 69360 Solaize France*

Abstract

Molybdenum disulfide (MoS_2) is considered one of the most likely materials that could be turned into low-cost hydrogen evolution reaction (HER) catalysts to replace noble metals in acidic solutions. However, several challenges prevent MoS_2 from being truly applicable, including limited number of active sites (typically only the edges are active) and poor conductivity. In this work, we perform an extensive density functional theory (DFT) screening of substitutional doping as a possibility to activate the otherwise inert basal surface. We assess 17 Earth abundant elements for molybdenum doping and 5 elements for sulfur substitution. Systematically determining the preference of the metallic dopants to be located on the edges rather than in the basal plane, we reveal that most dopants are much more likely to be incorporated at the edges, suggesting that advanced synthesis methods are required to obtain basal-plane doped catalysts. The latter may, however, feature many more active sites per MoS_2 formula unit, motivating our study on the properties of such substitutionally doped surfaces. For the first time for such a screening study, we explore not only the formation of H*, but also of OH* and H_2O* to explore the reactivity of the solvent. Two additional phenomena that could hinder the hydrogen production at these sites are investigated, namely H_2S release and the (local) segregation/dispersion tendency of the dopants in the basal surface. Moreover, to assess the electrocatalytic activity, we take the electrochemical potential explicitly into account via grand canonical DFT. Compared with pristine MoS_2 nanosheets, our results show that most doping elements significantly enhanced the electrocatalytic activity. Considering all assessed factors, we identify the most promising systems: Dimers of Ti, Zr and Hf and the substitution of S by P are predicted to lead to stable active sites on the basal plane with overpotentials of about 0.2 V.

Preprint submitted to Electrochimica Acta *July 19, 2022*

Keywords: Electrocatalysis, Substitutional doping, Hydrogen Evolution Reaction, Molybdenum disulfide

1. Introduction

Hydrogen production by water electrolysis is an intensely studied process for the medium-term storage of intermittent, decarbonized electricity such as solar, wind and tidal energy [1, 2]. Furthermore, "clean" hydrogen could also become a widely used energy vector for heavy transportation, replacing fossil fuels. However, the high cost of platinum electrodes represents one of the barriers towards the large-scale implementation of electrolytic generation of H_2 with the Proton Exchange Membrane (PEM) technology [3, 4].

In recent years, transition metal dichalcogenides (TMDs) with their intriguing structural and electronic properties have attracted increasing interest [5, 6, 7]. Their large-scale synthesis, based on the processes of liquid exfoliation, chemical vapor deposition and especially impregnation followed by sulfidation,[8] facilitates their use in various fields [9, 10]. The most important TMD is MoS_2, which has attracted great interest as a low-cost and environmentally friendly electrocatalyst for HER mechanism [11, 12, 13]. Furthermore, MoS_2 catalysts are already produced on large scales for hydrotreatment and hydro-cracking reactions for oil refining.

In general, the activity of the catalyst depends mainly on the total number of active sites and on their intrinsic activity. For pristine MoS_2, both theoretical calculations and subsequent experimental results have shown that promising sites are generally confined to the small region of exposed edges [14]. The predominantly exposed basal plane of the semi-conducting 2H-MoS_2 phase is, however, catalytically inactive in the absence of defects [15, 13].

Thus, the search for a method to activate the basal plane to exploit its large accessible surface area had led to extensive research. One of the many attempts focuses on the phase transformation of 2H to 1T polytype, which has promising sites on its basal plane but is metastable [16, 17, 18]. It was also reported that the 2H basal plane could be activated by the introduction of various types of defects and in particular sulfur vacancies [19, 20]. The conductivity of MoS_2 can also be improved by adding conductive supports such as metals and carbon materials [21, 22].

Substitutional doping, which is the main topic of our study, consists in replacing a small amounts of the original atoms (Mo/S) by other cations or

anions, respectively. Some dopants mainly change the nature of the MoS_2 edges (e.g., Co and Ni) [23], but are unlikely to change the HER mechanism and do not increase the number of sites [24]. The substitutional doping of MoS_2 can also improve the conductivity and create HER active sites on the basal plane by favoring vacancy and other defects formation[25, 26, 27]. Substitutional doping has already been explored to some extent in the experimental and theoretical literature for activating MoS_2 for HER: For instance, in a combined theoretical and experimental study Deng et al. have demonstrated that the HER activity of MoS_2 can be enhanced via single-atom Pt doping[28]. Similarly, DFT computations suggest that doping with other noble metals such as Ir, Pd, Rh, Au and Ag induce significant HER activities on the MoS_2 basal plane [29, 30, 31]. However, this does not completely avoid the use of noble metal precursors and is, therefore, not considered here. Experiments by Dai et al. reported that Co-doping of MoS_2 significantly improves the HER activity[32]. The origin of the improvement was not unambiguously identified, but improved electrical conductivity and increased defect densities were put forward as a possible explanation. A theoretical study suggested that Fe, Co, Ni and Cu dopants might increase the HER activity of either the basal plane, the edges or both.[33]. Subsequent, more detailed computations confirmed that these elements have advantages for the basal plane activity, but pointed out that the edges, which are much more easily doped than the basal plane, do not benefit from the doping.[34] Experimentally, however, doping by Fe, Co and Ni was reported not to have significant effects on HER, while Cu doping was found to lead to improved performances, although outperformed by Zn.[35] Zn doping was not only found to reduce the overpotential by 0.1 V, but also to decrease the Tafel slope from 101 mV dec^{-1} to 51 mV dec^{-1}. This significant enhancement was attributed to synergistic electronic and morphological effects, i.e., better conductivity and high number of active sites. Very recently, based on DFT computations, Ti doping was also suggested to be promising for increasing the HER activity.[36]

The substitutional doping of sulfur, rather than Mo, has also been tested. For example, Ye et al. showed the improvement of the catalytic activity of MoS_2 by preparing $MoS_2 - xP_x$ solid solutions [37]. Similarly, N was theoretically and experimentally found to tune the HER activity of MoS_2 both by generating additional active sites and by increasing the conductivity [38, 39]. It is to be noted that phosphorus doping might also "accidentally" originate from phosphate additives during the synthesis process of MoS_2.[40]

Isoelectronic dopants (such as Se and W) have also been tested. They are easier to incorporate but do not significantly change the electronic structure, so that only morphology related properties of MoS_2 are tuned, typically by increasing the number of active edge or basal plane defect sites.[41, 42]

All these reports are stimulating further engineering of MoS_2 via dopants to achieve high HER performance. However, synthetic issues (e.g., non-scalable synthesis, unwanted phases...) and lacking long-term stability have, so far, prevented the development of an MoS_2-based HER catalyst to be applicable on large scale [43] Therefore, identifying and understanding the impact of various dopants on the HER activity on MoS_2 remains an active topic.

In this work, we explore the influence on the HER activity of the basal plane of 2H-MoS_2 of substitutional metal-doping (17 non-noble metals) and/or non-metal doping (N, O, P, Se, Te) via an in silico screening. The primary criterion to classify them is the hydrogen adsorption energy ΔG_H, which should be close to 0 eV [44]. If ΔG_H is very negative, H will be strongly adsorbed and poison the catalyst surface, and if it is very positive, the Volmer step (adsorption of $H^+ + e^-$) might never occur. We consistently assess the tendency of the dopants to cluster together or to form single sites and determine the influence of this tendency on the catalytic properties. After an initial screening, we explicitly consider the electrochemical potential to study the reaction mechanism on promising sites, including the reactivity with water. This assessment, together with the determination of the stability of the doped basal planes with respect to H_2S-loss, and the impact of the dopants on the conductivity, provide a comprehensive overview on the prospects to induce catalytic activity on the defect free MoS_2 basal plane via substitutional doping.

2. Computational details

Density functional theory (DFT) computations were performed within the Vienna ab initio simulation package (VASP) [45]. Electron–ion interactions were modeled by projector augmented wave potentials. [46, 47] The generalized gradient approximation in the flavor of the dispersion corrected Perdew–Burke–Ernzerhof functional (PBE-dDsC) was applied to approximate exchange and correlation effects. [48, 49, 50] For the plane-wave basis set expansion, the cut-off energy was set to 500 eV. The precision setting of VASP is set to "accurate". The Brillouin zone is integrated by a Monkhorst

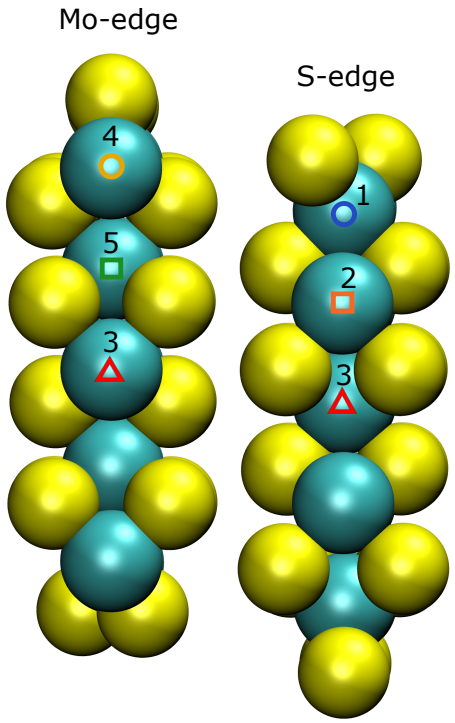

Figure 1: The different positions in the 50%S Mo-edge and the 50%S S-edge for the doping elements. The circles are the edges with blue (1) for the S edge and yellow (4) for the Mo edge, the squares orange (2) and green (5) are one layer after, and the triangles red (3) represent MoS_2 basal plane. The color code for atoms is yellow for S and greenish for Mo.

k-points mesh. For the description of the (doped) p(4×4) cell of the (0001) facet only the Γ-point was considered. For the edges, we adopted a $3 \times 3 \times 1$ k-point mesh. The convergence criterion for the self-consistency process is set to 10^{-5} eV for the optimization of the wave function. The maximum forces are converged to 0.025 eV during geometry optimization. Approximately 15 Å of vacuum is added both above and below the slabs in the z-direction [50].

For studying substitutional doping, we have assessed the energy difference between locating the dopant on the Mo- or S-edge compared to placing it in the basal plane. This is carried out with a fully relaxed symmetric six-layer p(1×2) edge model (see Figure 1).

Our first stage in the screening of substitutional doping of the basal plane consisted either the replacement of one sulfur atom by Y= N, O, P, Se, and Te or by replacing a triangle of molybdenum atoms by X= Ti, V, Cr, Mn,

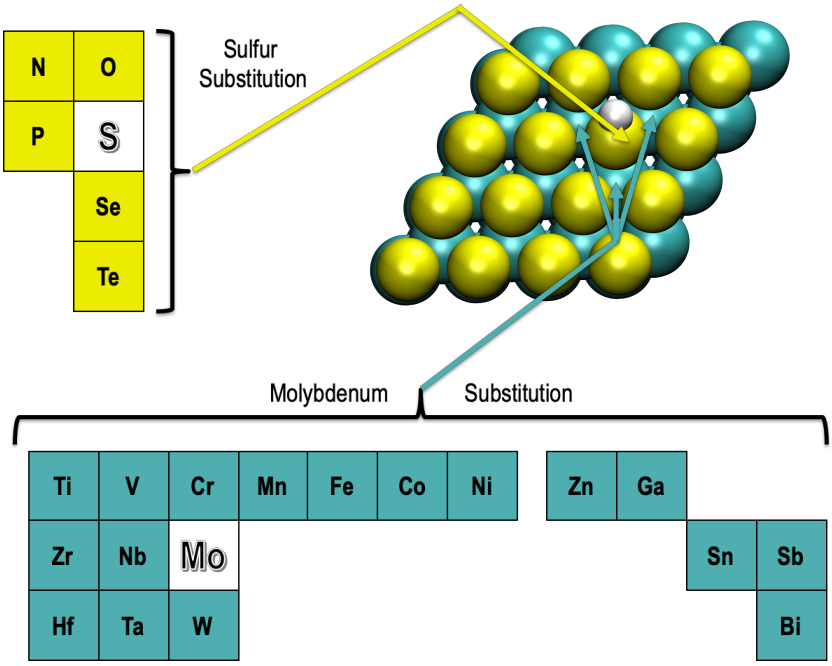

Figure 2: The different types of doping tested: S doping, Mo doping (monomer, dimer and trimer substitutions) and mixed doping (Mo+S).

Fe, Co, Ni, Zn, Ga, Zr, Nb, Sn, Sb, Hf, Ta, W and Bi. For X=[Cr, Mn, Fe, Co, Ni] we have considered spin polarization and tested various initial spins to identify the most stable magnetic state. For certain X and Y, we have also investigated a mixed doping denoted by X/Y (see Figure 2 for a schematic summary). For this first stage of the screening, the model system consists of 3 MoS_2 layers, with the lowest layer fixed in its bulk position and the dopants located in the top layer. We tried three doping densities (θ) defined as follows:

$$\theta = \frac{\text{number of doping atoms}}{\text{n(Mo)+n(S)}} \times 100 \tag{1}$$

Given the system size ($Mo_{48}S_{96}$), the doping density corresponds to to 0.69 %, 1.39 % and 2 % for 1X/S, 2X/S, and 3X/S, while only 0.69 % is tested for Mo/Y.

An important parameter is the tendency of dopants to either be dispersed in MoS_2 or to cluster together. To quantify this tendency, we determine the energy to break up dimers and trimers, ΔG_D and ΔG_T, respectively. Taking the fully dispersed model as a reference, we define:

$$\Delta G_D = \frac{1}{2} \times (2 \times E_{Mo_{47}X_1S_{96}} - E_{Mo_{48}S_{96}} - E_{Mo_{46}X_2S_{96}}) \tag{2}$$

and

$$\Delta G_T = \frac{1}{3} \times (3 \times E_{Mo_{47}X_1S_{96}} - 2 \times E_{Mo_{48}S_{96}} - E_{Mo_{45}X_3S_{96}}) \tag{3}$$

where X is the doping element.

The catalytic activity of all the mentioned structures is assessed by the hydrogen adsorption energy. For the basal planes, hydrogen is adsorbed on the "bent" position in agreement with previous studies [20]. The hydrogen adsorption energy (ΔG_H) is computed using the following equation:

$$\Delta G_H = E_H - E_{slab} - \frac{1}{2} \times G_{\mathrm{H_2}(g)} \tag{4}$$

where E_H and E_{slab} are the total energies of the system with and without hydrogen adsorbed on the active site, respectively, and G_{H_2} is the total energy of the hydrogen molecule: $G_{H_2(g)}$ = E(H_2) -TS where T is the room temperature (298.15 K) and S is the rotational and translational entropy at standard pressure. On selected systems, we have assessed the error of Eq. 4 compared to the "full" free energy treatment, where zero-point energy,

thermal vibrational effects and heat-capacity changes are fully accounted for (see Table S3). From this comparison, we conclude that the error incurred by the simplistic approximation is below 0.1 eV, similar to the uncertainty obtained by explicit DFT based molecular dynamics estimates.[51]. This accuracy is also well below our "uncertainty" threshold of about 0.5 eV for the identification of promising systems.

Considering ΔG_H and the relative stability of the dimers and trimers, we selected the promising structures to perform grand-canonical DFT computations. For these computations we rely on symmetric five layer structures ($Mo_{80}S_{160}$), where the central layer is frozen in its bulk geometry. For these systems, the doping densities are equal to 0.83 %, 1.67 % and 2.5 % for Mo and 0.83 % for S doping. These symmetric systems have been utilized to determine the potential dependent adsorption energy of H, OH and H_2O. For these grand-canonical DFT computations, the linearized Poisson-Boltzmann model as implemented in VASPsol is applied[52]. In VASPsol, the interface is defined as a function of the electron density, which is compared to a "critical" density, ρ_c. In line with our previous work[20] we set the iso-density value to to 0.00025 $e^-/\text{Å}^{-1}$. This is the same value as previously also used in the context of solvated alkali-metal ions [53, 54]. The Debye screening length is set to 3 Å, corresponding to a 1 M electrolyte. The potential dependence is studied by adapting the surface charge. Practically, the charge of the system is varied from -1 to $+1$ in steps of 0.2 e^-. The acquired connection between the grand-canonical energy and the electrochemical potential is then fitted to an analytical formula, which is a parabola for conductors and adapted to semi-conductors by accounting for the band-gap.[55, 56, 20]

For the grand-canonical DFT results, the adsorption energy ΔG_{ads} of the different species are calculated according to:

$$\Delta G_{ads}(U) = \frac{1}{2} \times (E_{tot}(U) - E_{slab}(U) - R) \tag{5}$$

where $E_{tot}(U)$ and $E_{slab}(U)$ are the potential-dependent energies of the symmetric MoS_2 surface with and without adsorbates, respectively. If the adsorbate is hydrogen (i.e., one hydrogen atom per surface), the reactant (R) is defined as:

$$R = 2 \times (H^+ + e^-) = 2\mu_H(U) = G_{\mathrm{H}_2(g)} - 2eU \tag{6}$$

where $G_{\mathrm{H}_2(g)}$ is the free energy of the hydrogen molecule, e is the elementary charge, and U is the applied potential with respect to the standard

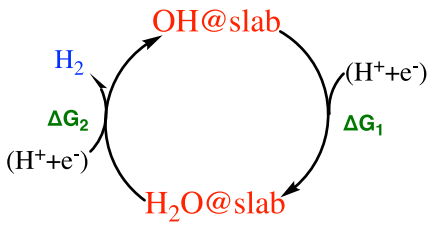

Figure 3: H_2 evolution via cycling between OH* and H_2O*. ΔG_1 corresponds to a Volmer step (adsorption of $H^+ + e- \rightarrow H*$), while ΔG_2 is a Heyrovsky step.

hydrogen electrode. This approach relies on the seminal paper introducing the computational hydrogen electrode, where Norskov and coworkers pointed out that the chemical potential of protons and electrons can be conveniently replaced by the one of a hydrogen molecule and a simple energy correction to account for the electrode potential.[57] Eq. 6 requires, in general, a pH dependence. Since we here study HER in acidic conditions, we assume a pH of 0 for which Eq. 6 is valid. For the adsorption of the water molecule, R $= 2G_{\mathrm{H_2O}}$ where $G_{\mathrm{H_2O}}$ is calculated similarly to $G_{\mathrm{H_2}(g)}$. The only difference is that the entropy contribution is divided by 2 to account the liquid state of H_2O.[58] For OH adsorption under the relevant reducing conditions, we set $R = 2G_{\mathrm{H_2O}} + 2(H^+ + e^-) - 2G_{\mathrm{H_2}}$ In other words, OH* is created by the adsorption of H_2O with a subsequent electro-reduction (formally a Heyrovsky step) that liberates H_2 ($\mathrm{H_2O + H^+ + e^- \longrightarrow OH\cdot + H_2}$), so that it formally should be considered as an adsorbed hydroxyl "radical" and not to be confused with adsorbed hydroxide "ion" OH^-. The adsorbed *OH can be an intermediate in HER (see Fig. 3), as long as its formation is exothermic and the corresponding reaction energies

$$\Delta G_1 = \frac{1}{2} \times (E_{tot}(\mathrm{H_2O}) - E_{tot}(\mathrm{OH}) - 2 \times (\mathrm{H^+ + e^-})) \tag{7}$$

$$\Delta G_2 = \frac{1}{2} \times (E_{tot}(\mathrm{OH}) + 2 \times G_{\mathrm{H_2}} - E_{tot}(\mathrm{H_2O}) - 2 \times (\mathrm{H^+ + e^-})) \tag{8}$$

are close to zero.

We also compute the electrical conductivity (σ) of the most promising doped systems using BoltzTraP2 [59], which solves the semiclassical Boltzmann transport equation under the constant relaxation time approximation.

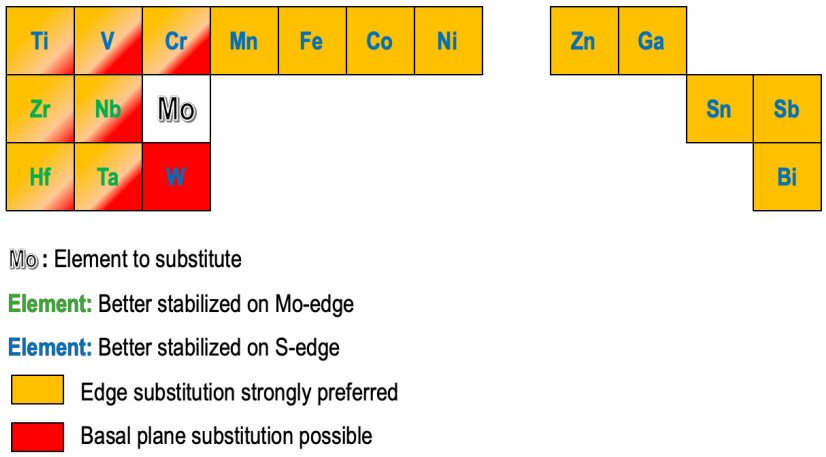

Figure 4: Stability of the dopants at the edges vs. the basal plane.

We obtain the electrical conductivity at 300 K around the Fermi energy level. This allows us to obtain a numerical estimate of the changes in conductivity upon doping.

3. Results and Discussion

The adsorption of H on the pristine basal plane of MoS_2 is unstable with a positive ΔG_H of up to 1.67 eV, while an ideal ΔG_H should be close to zero. We have explored two strategies to activate the inert basal plane: Curvature of MoS_2, modelled by nanotubes, and substitutional doping. However, since the activity of MoS_2 nanotubes is predicted to be disappointing, these results are only discussed in the SI (see section S1).

3.1. Relative Stability of Dopants at the Edge vs. the Basal Plane

Before turning to the basal plane, we first investigate the relative energy of placing dopants on the MoS_2 edge with respect to their location on the basal plane. In practice, we test five different positions, as shown Figure 1. The circles are the S and Mo edges, respectively, the squares are subsurface layer positions, and finally the (two symmetry equivalent) triangles represent MoS_2 basal plane. The relative stability of these different configurations are an indication of the preference of each dopant to be located at the edge or on

the basal plane. Figure S3 represents the detailed results for all dopants and positions tested, while Figure 4 provides a summary of the main findings. All dopants have an energetic preference for being located at the edges. However, the extent of this preference strongly depends on the particular metal. Most elements are stably located on the 50%S S-edge and only Nb, Zr, Hf and Ta are better stabilized on the 50%S Mo-edge. Nevertheless, experimentally it is well documented that many elements can be doped into the basal plane thanks to experimental techniques such as one-step sintering [39] and single-step hydrothermal reactions [60] leading to a good control of the amount and the position of the doped atoms. Hence, we have chosen a "critical" energy difference of 2 eV with respect to the most stable configuration: below this energy we expect that the substitutional doping should be feasible, while above the basal-plane doping seems largely compromised. We observe that only V, Nb, Ta, Cr and W are able to dope the MoS_2 basal plane with ΔE lower than 2 eV. Ti, Zr and Hf are also located close to this threshold and could, therefore, probably be doped in the basal plane as well. All other elements are strongly stabilized at the edges compared to the basal plane.

In view of the experimental reports of basal-plane doped MoS_2[61, 35, 37, 38] and the observation that the intrinsic activity of the edges is hard to improve[34] (i.e., edge-engineering mainly increases the number of active sites, not their thermodynamic overpotential), we investigate the large panel of non-noble metal dopants for activating the basal plane in the next section.

3.2. MoS_2 Basal Plane Doping

The geometry optimization of doped MoS_2 leads in most cases to a visible deformation. The most common deformation observed is a slight deviation from planarity as exemplified in Figure 5 a. In some cases, especially for large dopants (Bi, P, Sb) one of the sulfur atoms finds itself practically expelled from the surface (Fig. 5 b, c), while in the case of 3Ni/S a S-S dimer is formed (Fig. 5 d). Note that these geometries and others with adsorbed hydrogen are publicly available and additional geometries shown in the SI (see Fig. S5).

To select the most promising dopants, Computational Hydrogen Electrode (CHE)-based DFT calculations of the hydrogen adsorption energies are performed. Only for the promising dopants we perform the grand-canonical DFT computations for H, OH and H_2O adsorption. The influence of the number of substituted Mo was investigated by a systematic series of systems

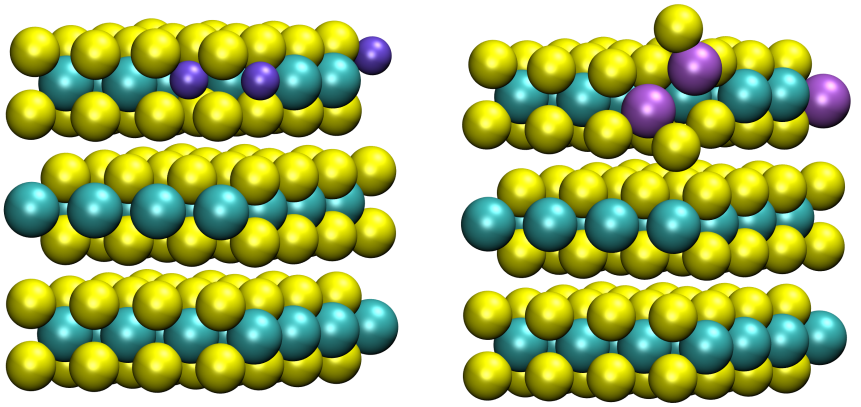

(a) 3Zn/S

(b) 3Sb/S

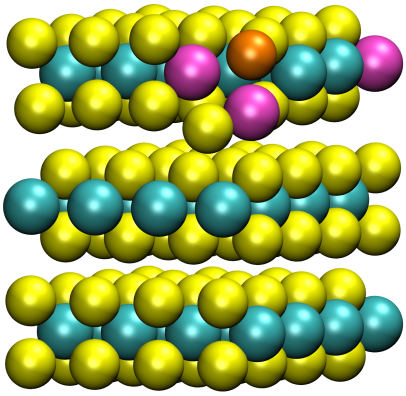

(c) 3Bi/P

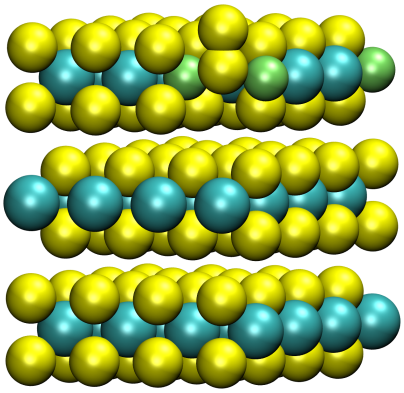

(d) 3Ni/S

Figure 5: The different deformations of MoS_2 basal plane after substitutional doping, but in the absence of hydrogen adsorption.

consisting in single-atom doping, dimer doping and a triangular trimer doping. The CHE results led to the exclusion of Cr and W, since ΔG_H was found to be very positive at all doping densities tested (the lowest ΔG_H value for Cr and W is 1.11 eV and 1.91 eV, respectively). For the other elements, the HER activity is significantly improved compared to the pristine basal plane. We distinguish three families depending on their interaction with H. The first features ΔG_H closest to 0 eV when θ= 2% (3Mn/S, 3Ni/S, 3V/S, 3Nb/S, 3Sn/S and 3Ta/S), the second when θ=1.39% (2Ti/S, 2Zr/S, 2Hf/S, 2Sb/S and 2Bi/S) and the third is when θ= 0.69% (1Co/S, 1Fe/S, 1Zn/S and 1Ga/S) (see Table S4). We also add to the list 3Ti/S, 3Zr/S and 3Hf/S as ΔG_H is very close to 0 eV for these systems (-0.12 eV, 0.17 eV and 0.2 eV respectively). Since the hydrogen adsorption energy strongly depends on the doping density, we determine the energy required to break up dimers and trimers (see Eq. 2 and 3, respectively) for all fourteen relevant dopants. Figure 6 depicts these reaction energies, with the single-atom dopant as the reference ($\Delta G_M = 0$, M: monoatomic). Lines connecting the energies have no physical meaning, but are added as a guide to the eye to facilitate the interpretation, i.e., whether or not a given dopant will tend to form "clusters" or is more stable as dispersed single-atoms in the basal plane.

When ΔG is negative, the dopant is found as a single atom in the basal plane, while a positive reaction indicates that cluster formation is thermodynamically likely. Three dopants show a uniform negative slope, indicating that single-atom doped MoS_2 is thermodynamically favored for V, Nb and Ta. Titanium, hafnium and zirconium show a weak preference for dimer formation. All the other dopants show a more (Ni) or less (Mn) pronounced tendency to cluster into trimers. This segregation tendency could indicate that metal-segregated hybrid structures would be obtained experimentally with most synthesis techniques. Thus, some of the structures mentioned above to be promising for HER according to ΔG_H are not favorable to be formed based on the results showed in Figure 6, in particular 3V/S, 3Nb/S, 3Ta/S, 2Sb/S, 2Bi/S, 1Co/S, 1Fe/S, 1Zn/S and 1Ga/S. In view of this additional "constraint" we have revised the list of systems that warrant a more detailed (grand-canonical DFT) investigation. In particular, we have added 3Zn/S, 3Bi/S, 2Sb/S, 2Ga/S, 1Nb/S and 1V/S.

The second type of doping is to substitute the sulfur atom. The tested elements are N, O, P, Se, and Te (see Table S5). For O, Se and Te, the adsorption energies of hydrogen are 1.1 eV, 2.0 eV and 1.9 eV, respectively. Hence, they clearly do not activate the basal plane. nitrogen and phospho-

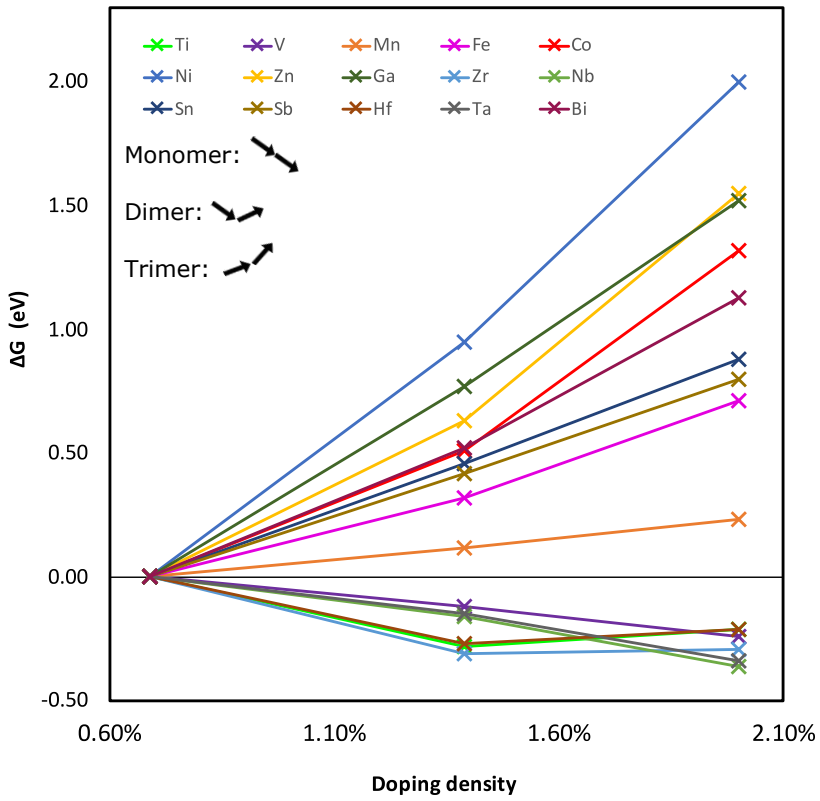

Figure 6: ΔG_M, ΔG_D and ΔG_T for each element and as a function of the different doping densities (0.69%, 1.39% and 2%). The arrows in the legend indicate the three typical behaviors leading to an energetic preference for monomers, dimers and trimers of the dopants.

rous, however, gave promising results with ΔG_H below 0 eV (-1.5 eV and -0.7 eV, respectively). As ΔG_H is very negative, we determined the adsorption energy for a second hydrogen atom. However, this second hydrogen atom is not bound (adsorption energies of 2.5 eV and 1.5 eV for Mo/N and Mo/P, respectively), in line with expected valencies of these group 15 elements. Despite the strong H adsorption, we will assess the interaction of these sites with water to determine if this might lead to HER active sites in analogy to some anti-site defects studied before.[20]

Finally, the mixed substitutional doping has been extensively explored. However, only few combinations turned out to be more interesting than the (conceptually simpler) single doped systems (see Table S6). In particular, 3Bi/P, 3Nb/P, 2Nb/P and 1Nb/P have been identified as sufficiently promising to be included in the more detailed grand-canonical DFT study below.

The possible mechanisms to produce H_2 at the promising active sites are Volmer-Heyrovsky if ΔG_H is close to 0 eV or Volmer-Tafel if ΔG_H is negative and a second hydrogen can be adsorbed. This second scenario is encountered for (3Zn, 3Sb, 3Bi, 3Ga, and 2Bi). However, upon the (exothermic) adsorption of the second hydrogen atom, all these cases lead to the release of H_2S. As a consequence an S-defect is created. While such defects might be catalytically active, they are beyond the scope of the present investigation that focuses on activating the basal plane in the absence of defects.

Given that HER is performed in aqueous electrolytes, we also assess the interaction of the potential active sites with H_2O an electrochemically formed OH. These species can either only weakly interact and thus be of no consequence for HER or they can "block" HER, typically forming stable surface OH* species or participate in HER, if oxygen is part of the active site and O-H bonds are easily broken and formed.

3.2.1. The influence of the electrochemical potential on the HER activity of the selected systems

Having identified the promising structures, we proceed to evaluate their HER activity by considering the influence of the electrochemical potential and the presence of other species, OH* and H_2O, since the presence of water at the electrochemical interface can have profound effects on the activity beyond the macroscopic effects captured by the Poisson-Boltzmann equation.[20] In the supporting information (see section S3) we display and discuss typical adsorption energy behaviors of H, OH and H_2O as a function of the electrochemical potential.

Figure 7 reports the relevant adsorption energies at the thermodynamic equilibrium potential for HER, i.e., 0 V vs SHE. Note, that these energies differ from the values for neutral surfaces used for the prescreening, since we are applying the grand-canonical DFT framework. The explicit inclusion of the electrochemical potential leads to an adjustment of the CHE results discussed above. Thus, we arrive at a new classification based on this more reliable level of theory. First, several systems (1V/S, 3Mn/S, 3Nb/S, 1Nb/S, 1Bi/S and 3Ta/S) feature $\Delta G_H(U)$ equal to or greater than 0.5 eV and are, thus no longer relevant for the typical HER mechanism (Fig. 7a). Since these sites seem unreactive with respect to H*, we did not consider OH* which tends to be less strongly adsorbed. Second, for 3Zn/S, 3Sb/S, 3Bi/S and 3Ga/S ΔG_H(U) is very negative (≤ -0.5 eV; see Fig 7b). However, these systems still suffer from the instability with respect to H_2S release. The last group of substitutional Mo doping is when ΔG_H(U) is close to 0 eV (Fig. 7c). This promising class of doped systems includes 3Ti/S, 2Ti/S, 3Ni/S, 1Co/S, 1Fe/S, 3V/S, 1Zn/S, 3Zr/S, 2Zr/S, 3Sn/S, 3Hf/S, 2Hf/S, 2Sb/S, 2Bi/S, and 1Ga/S. For these active sites the Volmer step is likely to occur at moderate over-potentials and, since the bonding is not strong, H_2 can be subsequently produced via a Heyrovsky step. However, these active sites might be blocked by OH*. As shown in Figure 7, we find that ΔG_{OH}(U) is positive for these active sites. Hence, OH* is not expected to block them. Furthermore, H_2O only interacts weakly with these surfaces, confirming the absence of strong interference of the solvent with HER, except for 3Ga/S where ΔG_{H_2O}(U) is -0.55 eV. In this particular case, the deformation of the surface exposes one of the Ga dopants, so that it can interact directly with the oxygen of the water molecule. We conclude that for these systems (except 3Ga/S) the promising sites are not blocked and the Volmer-Heyrovsky mechanism is possible at moderate overpotentials.

We now turn to the second type of doping, in which the sulfur atom is substituted, including mixed doping. We adsorb H, OH and H_2O. Figure 7d, shows that water adsorption remains thermoneutral. Hydrogen adsorption, however, is strongly exothermic for most cases. Niobium co-doped with phosphorus (1Nb/P, 2Nb/P and 3Nb/P) stabilizes a second adsorbed hydrogen, although not strongly enough to be relevant for HER. ΔG_H (0 V) is very close to 0 eV for 3Bi/P. Thus, the Volmer-Heyrovsky mechanism could occur on this particular active site. Similar to hydrogen adsorption, ΔG_{OH}(0 V) is negative for all systems except Mo/N. Consequently, OH* might block most of these sites, except when Volmer-Heyrovsky-type reaction mechanism in-

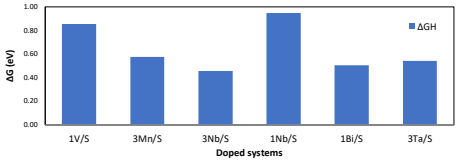

(a) First group: $\Delta G_H(0V) \geq 0.5$ eV

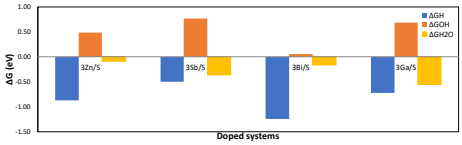

(b) Second group: $\Delta G_H(0V) \leq -0.5$ eV

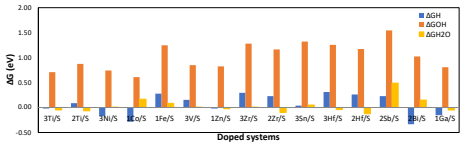

(c) Third group:-0.5 eV $< \Delta G_H(0V) <$ 0.5 eV

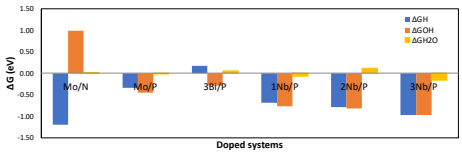

(d) Fourth group: Sulfur substitution

Figure 7: Comparison between the different ΔG values of H, OH and H_2O for each system and at 0 V vs SHE. (a), (b) and (c) are the molybdenum substitution and (d) is the sulfur substitution and mixed doping.

volving OH* and H_2O (see Figure 3) are favorable, which we explore in more detail in the next subsection.

3.2.2. Production of H_2 from adsorbed OH and H_2O

To assess the occurrence of H_2O/ OH cycles to generate H_2, we calculate ΔG_1 and ΔG_2 according to Eq. 7 and Eq. 8 as a function of the electrochemical potential. Only for three systems out of all the doped structures the formation of OH* is feasible and ΔG_1 and ΔG_2 are close to or smaller than 0 eV at overpotentials ≤ 0.5 V, namely Mo/P, 3Bi/S, and 3Bi/P with thermodynamic overpotentials η_{TD} equal to 0.2 V, 0.3 V and 0.5 V, respectively. Figure 8 illustrates the active site with the lowest thermodynamic overpotential in the series (0.2 V), namely Mo/P. Incidentally, this system is the one that is most likely to be achievable experimentally among the promising S-substituted systems.[37, 62]

3.2.3. Conductivity and identification of most promising systems

Grand-canonical DFT reveals the electronic structure of the various systems as either effectively metallic (e.g., H@2Zr/S following a parabola fit) or as semi-conducting (e.g., H@Mo/P which shows a piece-wise parabola on the reductive and oxidative side of the fundamental gap) as shown in Figure S4.

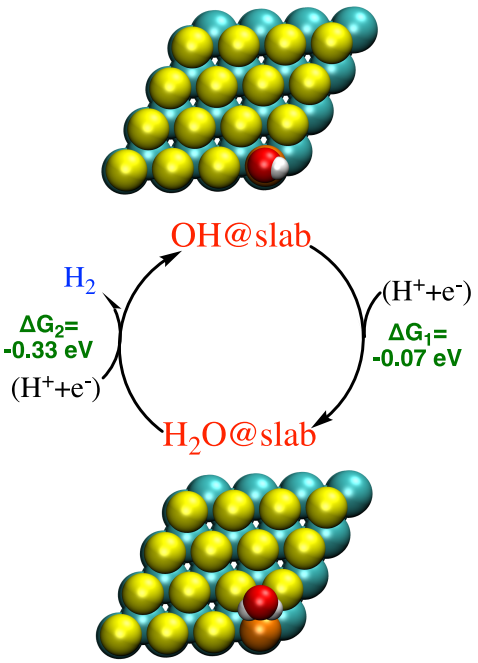

Figure 8: Different steps of the first cycle to produce H_2 from H_2O and OH* on Mo/P structure . The color code for atoms is white for H; red for O; orange for P; yellow for S and greenish for Mo.

However, this indirect probe of the electronic structure remains very qualitative. For selected systems we have computed the density of states (DOS). We observe that the gap of MoS_2 is significantly reduced in the presence of dopants. 2Zr/S, 2Ti/S and 2Hf/S feature a very similar DOS around the Fermi level (see Figure S7). In these systems that are promising for HER, the DOS around the Fermi-level is dominated by Mo atoms, suggesting that the dopant has not only a local effect on the electronic structure. This might explain why even one or two dopants are enough to activate the basal plane S atoms that are located above a site made up of three metallic atoms. In order to quantitatively estimate the conductivity of the promising doped systems, we resorted to the semi-classical transport equations as implemented in BoltzTraP2. The obtained electrical conductivities are summarized in the last column of Figure S8. Most of these doped systems are conductive, the exceptions being Mo/P and 3Ni/S. Hence, according to our computations, doping of the basal plane not only leads to novel active sites, but also lifts one of the major limitations of MoS_2 electrocatalysts, namely their low electrical conductivity.

Figure S8 summarizes the information from the various tests performed, including relative energies of placing dopants in the basal plane or at the edges and the tendency (or not) of dopants to cluster together. The release of H_2S and the geometrical distortion, especially upon H adsorption, are also summarized. Furthermore, all the relevant thermodynamic overpotentials, including at the OH* site, are reported. Based on these various criteria, we arrive at our final ranking: First of all, the considered site needs to produce H_2 at potentials $\geq$ -0.2 V vs SHE. Second, the corresponding mono-/dimer-/trimer doped system should be stable with respect to clustering/dispersion. Finally, doping of the basal plane compared to doping of the edge site should be relatively easy. As mentioned above, Mo/P releases H_2 via the OH/H_2O cycle at an overpotential as low as 0.2 V and is, thus, the most promising S-substituted electrocatalyst. From all the Mo substitutionally doped systems tested, only 2Ti/S, 2Zr/S and 2Hf/S are found to be truly promising, i.e., satisfying all three criteria. These sites generate H_2 via the Volmer-Heyrovsky mechanism. In order to further investigate the stability of these promising systems we have calculated the formation energy ΔE_f of Ti, Zr and Hf dimers. For all these systems, ΔE_f is negative (-0.70, -1.15 eV and -1.25 eV, respectively, see Table S7. Hence, to a first approximation one can expect that these dimers can be formed experimentally. We have also assessed the "dynamical" stability of these systems by ab initio molecular dynamics at 500

K, a temperature that is roughly representative for synthesis conditions. As shown in Fig. S9, the systems are stable over 30 ps. Given that ZrS_2 and HfS_2 have been reported as reasonable HER catalysts[63] and experiments indicate that doping with titanium and zirconium is possible in MoS_2,[64, 65] we expect that our predictions will spur corresponding experiments. Similarly, substitutional P doping of MoS_2 seems experimentally feasible[62] and our computations suggest that OH* species might not only be responsible for the experimentally observed increase in interlayer spacing, but also for the HER activity.

4. Conclusion

We have extensively (17 metals, 5 non-metals) studied substitutional doping of Mo and S in view of three complementary criteria: activity, feasibility and stability. The activity is assessed via hydrogen adsorption energies, with the promising systems being re-visited relying on grand-canonical DFT in order to account for the electrochemical potential. Furthermore, we have also quantified the improvement of the electrical conductivity of MoS_2 due to substitutional doping. The feasibility is addressed via two aspects: (a) relative stability of doping the edges vs. the basal plane and (b) the tendency of dopants to segregate (i.e. cluster). Finally, the stability of the proposed active sites is estimated by analyzing (a) the deformation induced by adsorbates, (b) release of H_2S under HER conditions and (c) "blocking" of active sites by OH* adsorption. OH* adsorption can, however, be seen as a modification of the active site that might still lead to HER, a possibility we have also assessed. Our computations identify 2Ti/S, 2Zr/S and 2Hf/S as the most promising subsitutional dopants in order to activate HER on the 2H basal plane of MoS_2 at overpotentials of about 0.2 V. For Mo/P, i.e. doping by phosphorus, the active site consists of OH*, but features a similarly low overpotential. Given our comprehensive analysis of substitutional doping and the few truly promising systems for activating the 2H basal plane of MoS_2 we expect to motivate experimental investigations to test these predictions.

Author Contributions

Nawras Abidi: Investigation, Writing - Original Draft Audrey Bonduelle-Skrzypczak: Writing - Review Stephan N. Steinmann: Supervision, Conceptualization, Resources, Writing - Review & Editing

Conflicts of interest

There are no conflicts to declare

Acknowledgements

This work was financially supported by Région Auvergne Rhône-Alpes through the project Pack Ambition Recherche 2018 MoSHi. We are very grateful to IFP Energies nouvelles for supporting the MoSHy project (N^o 1801167601) and to the IFP Energies nouvelles team, Mona Marie Obadia and Quentin Cacciuttolo, for discussing the MoS_2 solids that should meet the predictions of molecular modeling in the case of hydrogen production by water electrolysis. The authors thank the SYSPROD project and AXELERA Pôle de Compétitivité for financial support (PSMN Data Center).

Supporting Information

The supplementary material contains the results for hydrogen adsorption on MoS_2 nanotubes and additional Figures and Tables. Coordinates and DFT raw data is freely available on NOMAD-lab: https://dx.doi.org/10.17172/NOMAD/2022.04.11-1. The script to post-process VASP computations to GC-DFT is provided.

References

[1] J. A. Turner, Sustainable hydrogen production, Science 305 (5686) (2004) 972–974.

[2] M. Dresselhaus, I. Thomas, Alternative energy technologies, Nature 414 (6861) (2001) 332–337.

[3] J. Greeley, I. Stephens, A. Bondarenko, T. P. Johansson, H. A. Hansen, T. Jaramillo, J. Rossmeisl, I. Chorkendorff, J. K. Nørskov, Alloys of platinum and early transition metals as oxygen reduction electrocatalysts, Nature chemistry 1 (7) (2009) 552–556.

[4] J. Greeley, T. F. Jaramillo, J. Bonde, I. Chorkendorff, J. K. Nørskov, Computational high-throughput screening of electrocatalytic materials for hydrogen evolution, Nature materials 5 (11) (2006) 909–913.

[5] C. Tan, H. Zhang, Two-dimensional transition metal dichalcogenide nanosheet-based composites, Chemical Society Reviews 44 (9) (2015) 2713–2731.

[6] S. Manzeli, D. Ovchinnikov, D. Pasquier, O. V. Yazyev, A. Kis, 2d transition metal dichalcogenides, Nature Reviews Materials 2 (8) (2017) 17033.

[7] Z. W. Seh, J. Kibsgaard, C. F. Dickens, I. Chorkendorff, J. K. Nørskov, T. F. Jaramillo, Combining theory and experiment in electrocatalysis: Insights into materials design, Science 355 (6321) (2017) eaad4998.

[8] P. Munnik, P. E. de Jongh, K. P. de Jong, Recent Developments in the Synthesis of Supported Catalysts, Chem. Rev. 115 (14) (2015) 6687–6718. doi:10.1021/cr500486u.
URL https://doi.org/10.1021/cr500486u

[9] J. N. Coleman, M. Lotya, A. O'Neill, S. D. Bergin, P. J. King, U. Khan, K. Young, A. Gaucher, S. De, R. J. Smith, et al., Two-dimensional nanosheets produced by liquid exfoliation of layered materials, Science 331 (6017) (2011) 568–571.

[10] Y.-H. Lee, X.-Q. Zhang, W. Zhang, M.-T. Chang, C.-T. Lin, K.-D. Chang, Y.-C. Yu, J. T.-W. Wang, C.-S. Chang, L.-J. Li, et al., Synthesis of large-area mos2 atomic layers with chemical vapor deposition, Advanced materials 24 (17) (2012) 2320–2325.

[11] H. Tributsch, J. Bennett, Electrochemistry and photochemistry of mos2 layer crystals. i, Journal of Electroanalytical Chemistry and Interfacial Electrochemistry 81 (1) (1977) 97–111.

[12] P. Raybaud, J. Hafner, G. Kresse, S. Kasztelan, H. Toulhoat, Ab Initio Study of the H2–H2S/MoS2 Gas–Solid Interface: The Nature of the Catalytically Active Sites, Journal of Catalysis 189 (1) (2000) 129–146. doi:10.1006/jcat.1999.2698.
URL https://linkinghub.elsevier.com/retrieve/pii/S0021951799926982

[13] B. Hinnemann, P. G. Moses, J. Bonde, K. P. Jørgensen, J. H. Nielsen, S. Horch, I. Chorkendorff, J. K. Nørskov, Biomimetic hydrogen evolution: Mos2 nanoparticles as catalyst for hydrogen evolution, Journal of the American Chemical Society 127 (15) (2005) 5308–5309.

[14] T. F. Jaramillo, K. P. Jørgensen, J. Bonde, J. H. Nielsen, S. Horch, I. Chorkendorff, Identification of active edge sites for electrochemical h2 evolution from mos2 nanocatalysts, Science 317 (5834) (2007) 100–102.

[15] J. Bonde, P. G. Moses, T. F. Jaramillo, J. K. Nørskov, I. Chorkendorff, Hydrogen evolution on nano-particulate transition metal sulfides, Faraday discussions 140 (2009) 219–231.

[16] D. Voiry, H. Yamaguchi, J. Li, R. Silva, D. C. Alves, T. Fujita, M. Chen, T. Asefa, V. B. Shenoy, G. Eda, et al., Enhanced catalytic activity in strained chemically exfoliated ws 2 nanosheets for hydrogen evolution, Nature materials 12 (9) (2013) 850–855.

[17] M. A. Lukowski, A. S. Daniel, F. Meng, A. Forticaux, L. Li, S. Jin, Enhanced Hydrogen Evolution Catalysis from Chemically Exfoliated Metallic MoS2 Nanosheets, J. Am. Chem. Soc. 135 (28) (2013) 10274–10277. doi:10.1021/ja404523s.
URL https://doi.org/10.1021/ja404523s

[18] M. Chhowalla, H. S. Shin, G. Eda, L.-J. Li, K. P. Loh, H. Zhang, The chemistry of two-dimensional layered transition metal dichalcogenide nanosheets, Nature chemistry 5 (4) (2013) 263–275.

[19] H. Li, C. Tsai, A. L. Koh, L. Cai, A. W. Contryman, A. H. Fragapane, J. Zhao, H. S. Han, H. C. Manoharan, F. Abild-Pedersen, et al., Activating and optimizing mos 2 basal planes for hydrogen evolution through the formation of strained sulphur vacancies, Nature materials 15 (1) (2016) 48–53.

[20] N. Abidi, A. Bonduelle-Skrzypczak, S. N. Steinmann, Revisiting the active sites at the mos2/h2o interface via grand-canonical dft: The role of water dissociation, ACS applied materials & interfaces 12 (28) (2020) 31401–31410.

[21] X. Huang, Z. Zeng, S. Bao, M. Wang, X. Qi, Z. Fan, H. Zhang, Solution-phase epitaxial growth of noble metal nanostructures on dispersible single-layer molybdenum disulfide nanosheets, Nature communications 4 (1) (2013) 1–8.

[22] Y. Li, H. Wang, L. Xie, Y. Liang, G. Hong, H. Dai, Mos2 nanoparticles grown on graphene: an advanced catalyst for the hydrogen evolution

reaction, Journal of the American Chemical Society 133 (19) (2011) 7296–7299.

[23] M. Šarić, J. Rossmeisl, P. G. Moses, Modeling the active sites of Co-promoted MoS2 particles by DFT, Phys. Chem. Chem. Phys. 19 (3) (2017) 2017–2024. doi:10.1039/C6CP06881B.
URL http://pubs.rsc.org/en/content/articlelanding/2017/cp/c6cp06881b

[24] C. Tsai, F. Abild-Pedersen, J. K. Nørskov, Tuning the MoS2 Edge-Site Activity for Hydrogen Evolution via Support Interactions, Nano Lett. 14 (3) (2014) 1381–1387. doi:10.1021/nl404444k.
URL https://doi.org/10.1021/nl404444k

[25] Q. Yue, S. Chang, S. Qin, J. Li, Functionalization of monolayer mos2 by substitutional doping: a first-principles study, Physics Letters A 377 (19-20) (2013) 1362–1367.

[26] K. Dolui, I. Rungger, C. Das Pemmaraju, S. Sanvito, Possible doping strategies for MoS${}_{2}$ monolayers: An ab initio study, Phys. Rev. B 88 (7) (2013) 075420. doi:10.1103/PhysRevB.88.075420.
URL https://link.aps.org/doi/10.1103/PhysRevB.88.075420

[27] Y. Kang, Interplay between transition-metal dopants and sulfur vacancies in MoS2 electrocatalyst, Surface Science 704 (2021) 121759. doi:10.1016/j.susc.2020.121759.
URL https://www.sciencedirect.com/science/article/pii/S0039602820307238

[28] J. Deng, H. Li, J. Xiao, Y. Tu, D. Deng, H. Yang, H. Tian, J. Li, P. Ren, X. Bao, Triggering the electrocatalytic hydrogen evolution activity of the inert two-dimensional MoS $_2$ surface via single-atom metal doping, Energy & Environmental Science 8 (5) (2015) 1594–1601. doi:10.1039/C5EE00751H.
URL http://xlink.rsc.org/?DOI=C5EE00751H

[29] G. Gao, Q. Sun, A. Du, Activating catalytic inert basal plane of molybdenum disulfide to optimize hydrogen evolution activity via defect doping and strain engineering, The Journal of Physical Chemistry C 120 (30) (2016) 16761–16766.

[30] Z. Zhang, K. Chen, Q. Zhao, M. Huang, X. Ouyang, Electrocatalytic and photocatalytic performance of noble metal doped monolayer

MoS2 in the hydrogen evolution reaction: A first principles study, Nano Materials Science 3 (1) (2021) 89–94. doi:10.1016/j.nanoms.2020.05.001. URL https://www.sciencedirect.com/science/article/pii/S2589965120300234

[31] Y. Rui, S. Zhang, X. Shi, X. Zhang, R. Wang, X. Li, Chemically Activating Tungsten Disulfide via Structural and Electronic Engineering Strategy for Upgrading the Hydrogen Evolution Reaction, ACS Appl. Mater. Interfaces 13 (42) (2021) 49793–49801. doi:10.1021/acsami.1c10714. URL https://doi.org/10.1021/acsami.1c10714

[32] X. Dai, K. Du, Z. Li, M. Liu, Y. Ma, H. Sun, X. Zhang, Y. Yang, Co-doped mos2 nanosheets with the dominant comos phase coated on carbon as an excellent electrocatalyst for hydrogen evolution, ACS applied materials & interfaces 7 (49) (2015) 27242–27253.

[33] H. Wang, C. Tsai, D. Kong, K. Chan, F. Abild-Pedersen, J. K. Nørskov, Y. Cui, Transition-metal doped edge sites in vertically aligned mos 2 catalysts for enhanced hydrogen evolution, Nano Research 8 (2) (2015) 566–575.

[34] M. Hakala, R. Kronberg, K. Laasonen, Hydrogen adsorption on doped mos 2 nanostructures, Scientific reports 7 (1) (2017) 1–13.

[35] Y. Shi, Y. Zhou, D.-R. Yang, W.-X. Xu, C. Wang, F.-B. Wang, J.-J. Xu, X.-H. Xia, H.-Y. Chen, Energy level engineering of mos2 by transition-metal doping for accelerating hydrogen evolution reaction, Journal of the American Chemical Society 139 (43) (2017) 15479–15485.

[36] W. Shi, Z. Wang, Titanium-doped mos2 monolayer as highly efficient catalyst for hydrogen evolution reaction, in: IOP Conference Series: Earth and Environmental Science, Vol. 558, IOP Publishing, 2020, p. 032048.

[37] R. Ye, P. del Angel-Vicente, Y. Liu, M. J. Arellano-Jimenez, Z. Peng, T. Wang, Y. Li, B. I. Yakobson, S.-H. Wei, M. J. Yacaman, et al., High-performance hydrogen evolution from mos2 (1–x) p x solid solution, Advanced Materials 28 (7) (2016) 1427–1432.

[38] W. Zhou, D. Hou, Y. Sang, S. Yao, J. Zhou, G. Li, L. Li, H. Liu, S. Chen, Moo 2 nanobelts@ nitrogen self-doped mos 2 nanosheets as effective

electrocatalysts for hydrogen evolution reaction, Journal of Materials Chemistry A 2 (29) (2014) 11358–11364.

[39] W. Xiao, P. Liu, J. Zhang, W. Song, Y. P. Feng, D. Gao, J. Ding, Dual-functional n dopants in edges and basal plane of mos2 nanosheets toward efficient and durable hydrogen evolution, Advanced Energy Materials 7 (7) (2017) 1602086.

[40] J. A. Bergwerff, T. Visser, G. Leliveld, B. D. Rossenaar, K. P. de Jong, B. M. Weckhuysen, Envisaging the Physicochemical Processes during the Preparation of Supported Catalysts: Raman Microscopy on the Impregnation of Mo onto Al2O3 Extrudates, J. Am. Chem. Soc. 126 (44) (2004) 14548–14556. doi:10.1021/ja040107c.
URL https://doi.org/10.1021/ja040107c

[41] X. Ren, Q. Ma, H. Fan, L. Pang, Y. Zhang, Y. Yao, X. Ren, S. F. Liu, A Se-doped MoS2 nanosheet for improved hydrogen evolution reaction, Chem. Commun. 51 (88) (2015) 15997–16000. doi:10.1039/C5CC06847A.
URL https://pubs.rsc.org/en/content/articlelanding/2015/cc/c5cc06847a

[42] J. N. He, Y. Q. Liang, J. Mao, X. M. Zhang, X. J. Yang, Z. D. Cui, S. L. Zhu, Z. Y. Li, B. B. Li, 3D Tungsten-Doped MoS $_2$ Nanostructure: A Low-Cost, Facile Prepared Catalyst for Hydrogen Evolution Reaction, J. Electrochem. Soc. 163 (5) (2016) H299–H304. doi:10.1149/2.0841605jes.
URL https://iopscience.iop.org/article/10.1149/2.0841605jes

[43] C. Meng, X. Chen, Y. Gao, Q. Zhao, D. Kong, M. Lin, X. Chen, Y. Li, Y. Zhou, Recent modification strategies of mos2 for enhanced electrocatalytic hydrogen evolution, Molecules 25 (5) (2020) 1136.

[44] J. K. Nørskov, T. Bligaard, A. Logadottir, J. Kitchin, J. G. Chen, S. Pandelov, U. Stimming, Trends in the exchange current for hydrogen evolution, Journal of The Electrochemical Society 152 (3) (2005) J23.

[45] G. Kresse, J. Furthmüller, Efficiency of ab-initio total energy calculations for metals and semiconductors using a plane-wave basis set, Computational Materials Science 6 (1) (1996) 15–50. doi:10.1016/0927-0256(96)00008-0.

[46] P. E. Blochl, Projector augmented-wave method, Phys. Rev. B 50 (1994) 17953.

[47] G. Kresse, D. Joubert, From ultrasoft pseudopotentials to the projector augmented-wave method, Phys. Rev. B 59 (1999) 1758.

[48] J. P. Perdew, K. Burke, M. Ernzerhof, Generalized gradient approximation made simple, Physical review letters 77 (18) (1996) 3865.

[49] S. N. Steinmann, C. Corminboeuf, Comprehensive benchmarking of a density-dependent dispersion correction, Journal of chemical theory and computation 7 (11) (2011) 3567–3577.

[50] S. N. Steinmann, P. Sautet, C. Michel, Solvation free energies for periodic surfaces: comparison of implicit and explicit solvation models, Physical Chemistry Chemical Physics 18 (46) (2016) 31850–31861. doi:10.1039/c6cp04094b.

[51] R. Réocreux, C. Michel, P. Fleurat-Lessard, P. Sautet, S. N. Steinmann, Evaluating Thermal Corrections for Adsorption Processes at the Metal/Gas Interface, Journal of Physical Chemistry C 123 (47) (2019) 28828–28835. doi:10.1021/acs.jpcc.9b09863.

[52] K. Mathew, V. S. C. Kolluru, S. Mula, S. N. Steinmann, R. G. Hennig, Implicit self-consistent electrolyte model in plane-wave density-functional theory, J. Chem. Phys. 151 (23) (2019) 234101. doi:10.1063/1.5132354.
URL `https://aip.scitation.org/doi/abs/10.1063/1.5132354`

[53] S. N. Steinmann, C. Michel, R. Schwiedernoch, P. Sautet, Impacts of electrode potentials and solvents on the electroreduction of CO2: A comparison of theoretical approaches, Physical Chemistry Chemical Physics 17 (21) (2015) 13949–13963. doi:10.1039/c5cp00946d.
URL `http://dx.doi.org/10.1039/C5CP00946D`

[54] N. Lespes, J. S. Filhol, Using Implicit Solvent in Ab Initio Electrochemical Modeling: Investigating Li+/Li Electrochemistry at a Li/Solvent Interface, Journal of Chemical Theory and Computation 11 (7) (2015) 3375–3382. doi:10.1021/acs.jctc.5b00170.

[55] Y. M. Hajar, L. Treps, C. Michel, E. A. Baranova, S. N. Steinmann, Theoretical insight into the origin of the electrochemical promotion of ethylene oxidation on ruthenium oxide, Catalysis Science and Technology 9 (21) (2019) 5915–5926. doi:10.1039/c9cy01421g.

[56] A. Curutchet, P. Colinet, C. Michel, S. N. Steinmann, T. Le Bahers, Two-sites are better than one: revisiting the oer mechanism on coooh by dft with electrode polarization, Physical Chemistry Chemical Physics 22 (13) (2020) 7031–7038.

[57] J. K. Nørskov, J. Rossmeisl, A. Logadottir, L. Lindqvist, J. R. Kitchin, T. Bligaard, H. Jonsson, Origin of the overpotential for oxygen reduction at a fuel-cell cathode, The Journal of Physical Chemistry B 108 (46) (2004) 17886–17892.

[58] P. Wang, S. N. Steinmann, G. Fu, C. Michel, P. Sautet, Key Role of Anionic Doping for H2 Production from Formic Acid on Pd(111), ACS Catal. 7 (3) (2017) 1955–1959. doi:10.1021/acscatal.6b03544.
URL https://doi.org/10.1021/acscatal.6b03544

[59] G. K. Madsen, J. Carrete, M. J. Verstraete, Boltztrap2, a program for interpolating band structures and calculating semi-classical transport coefficients, Computer Physics Communications 231 (2018) 140–145.

[60] W. Qiao, W. Xu, X. Xu, L. Wu, S. Yan, D. Wang, Construction of active orbital via single-atom cobalt anchoring on the surface of 1t-mos2 basal plane toward efficient hydrogen evolution, ACS Applied Energy Materials 3 (3) (2020) 2315–2322.

[61] J. Deng, H. Li, J. Xiao, Y. Tu, D. Deng, H. Yang, H. Tian, J. Li, P. Ren, X. Bao, Triggering the electrocatalytic hydrogen evolution activity of the inert two-dimensional mos 2 surface via single-atom metal doping, Energy & environmental science 8 (5) (2015) 1594–1601.

[62] P. Liu, J. Zhu, J. Zhang, P. Xi, K. Tao, D. Gao, D. Xue, P Dopants Triggered New Basal Plane Active Sites and Enlarged Interlayer Spacing in MoS2 Nanosheets toward Electrocatalytic Hydrogen Evolution, ACS Energy Lett. 2 (4) (2017) 745–752. doi:10.1021/acsenergylett.7b00111.
URL https://doi.org/10.1021/acsenergylett.7b00111

[63] R. J. Toh, Z. Sofer, M. Pumera, Catalytic properties of group 4 transition metal dichalcogenides (mx 2; m= ti, zr, hf; x= s, se, te), Journal of Materials Chemistry A 4 (47) (2016) 18322–18334.

[64] J. Radhakrishnan, K. Biswas, Facile synthesis of Ti doped MoS2 and its superior adsorption properties, Materials Letters 280 (2020) 128522. doi:10.1016/j.matlet.2020.128522.
URL https://www.sciencedirect.com/science/article/pii/S0167577X20312283

[65] M. Ikram, R. Tabassum, U. Qumar, S. Ali, A. Ul-Hamid, A. Haider, A. Raza, M. Imran, S. Ali, Promising performance of chemically exfoliated Zr-doped MoS2 nanosheets for catalytic and antibacterial applications, RSC Adv. 10 (35) (2020) 20559–20571. doi:10.1039/D0RA02458A.
URL http://pubs.rsc.org/en/content/articlelanding/2020/ra/d0ra02458a